

## Entropy Generation for Flow and Heat Transfer of Sisko-Fluid Over an Exponentially Stretching Surface

Mohamed Abd El-Aziz<sup>1,2</sup> and A. M. Aly<sup>1,3,\*</sup>

**Abstract:** In the present study, the effects of the magnetic field on the entropy generation during fluid flow and heat transfer of a Sisko-fluid over an exponentially stretching surface are considered. The similarity transformations are used to transfer the governing partial differential equations into a set of nonlinear-coupled ordinary differential equations. Runge-Kutta-Fehlberg method is used to solve the governing problem. The effects of magnetic field parameter  $M$ , local slip parameter  $\lambda$ , generalized Biot number  $\gamma$ , Sisko fluid material parameter  $A$ , Eckert number  $Ec$ , Prandtl number  $Pr$  and Brinkman number  $Br$  at two values of power law index on the velocity, temperature, local entropy generation number  $N_G$  and Bejan number  $Be$  are inspected. Moreover, the tabular forms for local skin friction coefficient and local Nusselt number under the effects of the physical parameters are exhibited. The current results are helpful in checking the entropy generation for Sisko-fluid. It is found that, an extra magnetic field parameter makes higher Lorentz force that suppresses the velocity. For shear thinning fluids ( $n < 1$ ), the temperature dominates and the velocity rises. Local entropy generation number is more for larger generalized Biot number, magnetic field parameter and Brinkman number. The local skin friction coefficient increases as magnetic field parameter and material parameter are increase and it decreases as local slip parameter increases. The local Nusselt number decreases as magnetic field parameter, local slip parameter and Eckert number are increase, while it increases as material parameter, generalized Biot number and Prandtl number are increase.

**Keywords:** Boundary layer, entropy generation, exponentially stretching surface, magnetic field, sisko-fluid.

### 1 Introduction

The non-Newtonian fluids are subsisting in the nature with wide range of industrial applications. Hence, there are numerous models for studying the physical properties of the non-Newtonian fluids. One of this model is power-law, in which the fluid properties can be predicted in power law region only. Nevertheless, the power law fails to analyze flow characteristics when shear rate become very small or large. Hence, Sisko [Sisko

---

<sup>1</sup> Department of Mathematics, Faculty of Science, King Khalid University, Abha, 61411, Saudi Arabia.

<sup>2</sup> Department of Mathematics, Faculty of Science, Helwan University, Helwan-Cairo, 11795, Egypt.

<sup>3</sup> Department of Mathematics, Faculty of Science, South Valley University, Qena, 83523, Egypt.

\*Corresponding Author: A. M. Aly. Email: abdelreham.abdallah@sci.svu.edu.eg; m\_abdelaziz999@yahoo.com.

(1958)] proposed Sisko fluid model to predict the fluid properties in power law region and at high shear rate. In the literature, Ali et al. [Ali, Zaman and Sajid (2014)] used Sisko model to describe the rheology of blood. Tanveer et al. [Tanveer, Hayat, Alsaedi et al. (2017)] investigated the peristaltic flow of Sisko material in curved channel. Khan et al. [Khan, Munawar and Abbasbandy (2010)] studied the heat transfer of a Sisko fluid in an annular pipe. Mekheimer et al. [Mekheimer and El Kot (2012)] studied the effects of the chemical reactions on the flow of Sisko fluid through an anisotropically tapered elastic arteries with overlapping stenosis. Nadeem et al. [Nadeem and Akbar (2010)] studied an incompressible Sisko fluid in the uniform inclined tube. Khan et al. [Khan, Qayyum, Hayat et al. (2018)] considered the entropy generation for boundary layer flow of Sisko fluid. Khan et al. [Khan, Khan, Alshomrani et al. (2016)] investigated the double-diffusive models on flow of Sisko fluid over a nonlinear stretching surface.

In addition, due to the importance of the heat transfer over stretching surface in the field of chemical engineering, metallurgy, and production of papers. Hence, the boundary layer flow and heat transfer over a stretching surface has gained much importance in the recent years [Bataller (2008); Mansour, El-Anssary and Aly (2008); Chamkha and Aly (2010); Chamkha, Aly and Al-Mudhaf (2010); Chamkha, Aly and Mansour (2011); Bachok, Ishak and Pop (2012); Hayat, Shafiq, Alsaedi et al. (2013); Ibrahim, Shankar and Nandeppanavar (2013); Ahmed, Aly and Mansour (2015); Abd El-Aziz and Afify (2016); Afify and Abd El-Aziz (2017); Raizah (2017)]. Abd El-Aziz et al. [Abd El-Aziz and Afify (2016); Afify and Abd El-Aziz (2017)] used Lie group method to analysis the heat transfer of non-Newtonian nanofluid over a stretching surface. Saleem et al. [Saleem and Abd El-Aziz (2019)] studied the entropy generation of radiated non-Newtonian power-law fluid past an exponentially moving surface. Abd El-Aziz et al. [Abd El-Aziz and Saleem (2019)] investigated the entropy generation of a Power-Law flow over a permeable exponential stretched surface with variable heat source and heat flux.

There are many applications such as MHD generators, nuclear reactors and geothermal energy extractions from MHD flow. Sparrow et al. [Sparrow and Cess (1961)] studied the effects of magnetic field on the natural convection heat transfer. Later, there are many attempts on studying the effects of magnetic field on the boundary layer flow and heat transfer over different geometries [Chamkha and Aly (2010); Chamkha, Mansour and Aly (2011); Uddin, Khan and Ismail (2012); Hayat, Shafiq, Alsaedi et al. (2013); Ibrahim, Shankar and Nandeppanavar (2013); Mabood, Khan and Ismail (2015); Hsiao (2016); Ghadikolaei, Hosseinzadeh and Ganji (2018); Krishna and Reddy (2018)]. Few recent studies about entropy generation for Sisko fluid can be seen via Hayat et al. [Hayat, Khan, Qayyum et al. (2018); Khan, Hayat, Alsaedi et al. (2018); Khan, Qayyum, Hayat et al. (2018)].

This study is mainly focus on the entropy generation during fluid flow and heat transfer of a Sisko-fluid over an exponentially stretching surface under the effects of the magnetic field. The similarity transformations are used to transfer the governing partial differential equations into a set of nonlinear-coupled ordinary differential equations. Runge-Kutta-Fehlberg method is used to solve the governing problem. It is found that, an extra magnetic field parameter makes higher Lorentz force that suppresses the velocity. For shear thinning fluids ( $n < 1$ ), the temperature dominates and the velocity rises. Local

entropy generation number is more for larger generalized Biot number  $\gamma$ , magnetic field parameter  $M$  and Brinkman number  $Br$ .

**2 Problem formulation**

The two-dimensional steady MHD boundary layer flow of a Sisko-fluid over an exponentially stretching surface is considered. At its lower surface, the sheet is heated convectively with temperature  $T_f$  and a heat transfer coefficient  $h_f$ . The uniform ambient temperature is  $T_\infty$ . Fig. 1 presents the initial schematic diagram of the current problem. Here, the  $x$ -axis is taken along the exponentially stretching surface and  $y$ -axis is normal to it. As shown in this figure, the transverse non-uniform magnetic field with strength  $B = B_0 e^{x/2L}$  is taken as parallel to the  $y$ -axis.

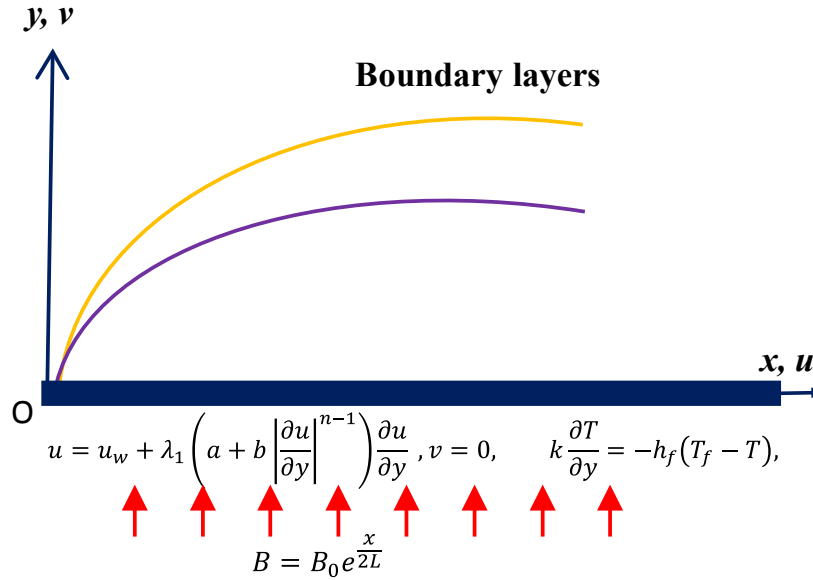


**Figure 1:** Initial schematic diagram of the problem

The governing equations are:

$$\frac{\partial u}{\partial x} + \frac{\partial v}{\partial y} = 0, \tag{1}$$

$$u \frac{\partial u}{\partial x} + v \frac{\partial u}{\partial y} = \frac{a}{\rho} \frac{\partial^2 u}{\partial y^2} + \frac{b}{\rho} \frac{\partial}{\partial y} \left( \left| \frac{\partial u}{\partial y} \right|^{n-1} \frac{\partial u}{\partial y} \right) - \frac{\sigma B^2}{\rho} u \tag{2}$$

$$u \frac{\partial T}{\partial x} + v \frac{\partial T}{\partial y} = \alpha \frac{\partial^2 T}{\partial y^2} + \frac{\sigma B^2}{\rho c_p} u^2 + \frac{a}{\rho c_p} \frac{\partial^2 u}{\partial y^2} + \frac{b}{\rho c_p} \left| \frac{\partial u}{\partial y} \right|^{n+1} \tag{3}$$

The imposed boundary conditions are:

$$u = u_w + \lambda_1 \left( a + b \left| \frac{\partial u}{\partial y} \right|^{n-1} \right) \frac{\partial u}{\partial y}, v = 0, \quad k \frac{\partial T}{\partial y} = -h_f (T_f - T), \tag{4}$$

$u \rightarrow 0, \quad T \rightarrow T_\infty$  as  $y \rightarrow \infty$

Introducing the following similarity transformations:

$$\psi = \left( \frac{2bLU_o^{2n-1}}{\rho} \right)^{\frac{1}{n+1}} e^{\frac{(2n-1)x}{(n+1)L}} f(\eta), \quad \eta = y \left( \frac{\rho U_o^{2-n}}{2bL} \right)^{\frac{1}{n+1}} e^{\frac{(2-n)x}{(n+1)L}} \quad (5)$$

$$T_f = T_\infty + T_0 e^{2x/L}, \quad B = B_0 e^{x/2L}$$

Then, the velocity components are:

$$u = \frac{\partial \psi}{\partial y} = U_o e^{\frac{x}{L}} f'(\eta), \quad (6)$$

$$v = -\frac{\partial \psi}{\partial x} = -\left( \frac{2bU_o^{2n-1}}{\rho L^n} \right)^{\frac{1}{n+1}} e^{\frac{(2n-1)x}{(n+1)L}} \left( \left( \frac{2n-1}{n+1} \right) f(\eta) + \left( \frac{2-n}{n+1} \right) \eta f'(\eta) \right)$$

The dimensionless forms of the governing equations are:

$$A f'''' + \frac{n}{2} |f''|^{n-1} f'''' + \left( \frac{2n-1}{n+1} \right) f f'' - f'^2 - M f' = 0, \quad (7)$$

$$\frac{1}{Pr} \theta'' + \left( \frac{2n-1}{n+1} \right) f \theta' - 2f' \theta + M Ec f'^2 + Ec \left[ A (f''')^2 + \frac{1}{2} |f''|^{n+1} \right] = 0, \quad (8)$$

With the boundary conditions:

$$f'(0) = 1 + \lambda(2A + |f''(0)|^{n-1}) f''(0), \quad f(0) = 0, \quad \theta'(0) = -\gamma(1 - \theta(0)), \quad (9)$$

$$f'(\infty) \rightarrow 0, \quad \theta(\infty) \rightarrow 0.$$

where,  $A = \frac{(Re_b/2)^{\frac{2}{n+1}}}{Re_a}$  is material parameter with  $Re_b = \frac{\rho u_w^{(2-n)} L^n}{b}$ ,  $Re_a = \frac{\rho u_w L}{a}$ .

$B = B_0 e^{\frac{x}{2L}}$  is the applied magnetic field,  $M = \frac{\sigma B_0^2 L}{\rho U_o}$  is magnetic field parameter,

$Pr = \frac{u_w L}{\alpha} \left( \frac{Re_b}{2} \right)^{\frac{-2}{n+1}}$  is the Prandtl number,  $Ec = \frac{u_w^2}{\Delta T c_p} = \frac{u_0^2}{T_0 c_p}$  is the Eckert number and

$\lambda = \frac{\lambda_1 b u_w^{(n-1)}}{L^n} \left( \frac{Re_b}{2} \right)^{\frac{n}{n+1}}$  is the local slip parameter and  $\gamma = \frac{h_f L}{k} \left( \frac{Re_b}{2} \right)^{\frac{1}{n+1}}$  is the generalized Biot number.

The skin friction coefficient and local Nusselt number are given by:

$$C_{fx} = \frac{2\tau_w}{\rho_f u_w^2}, \quad \tau_w = \left( a + b \left| \frac{\partial u}{\partial y} \right|^{n-1} \right) \frac{\partial u}{\partial y} \Big|_{y=0} \quad (10)$$

$$C_{fx} \left( \frac{Re_b}{2} \right)^{\frac{1}{n+1}} = 2A f''(0) + |f''(0)|^{n-1} f''(0)$$

$$Nu_x = \frac{-L}{T_f - T_\infty} \left( \frac{\partial T}{\partial y} \right)_{y=0} = - \left( \frac{Re_b}{2} \right)^{\frac{1}{n+1}} \theta'(0) \quad (11)$$

$$Nu_x \left( \frac{Re_b}{2} \right)^{\frac{-1}{n+1}} = -\theta'(0) \quad (12)$$

where,  $q_w = -k \left( \frac{\partial T}{\partial y} \right)_{y=0}$  is the surface heat flux,  $\tau_w$  is the shear stress along the stretching surface.

### 3 Entropy generation

In this study, we considered the Sisko-fluid, so the volumetric form of irreversibility in flow by exponentially stretching surface is defined as:

$$S_G = \frac{k}{T_\infty} \left( \frac{\partial T}{\partial y} \right)^2 + \frac{1}{T_\infty} \left( a \left( \frac{\partial u}{\partial y} \right)^2 + b \left| \frac{\partial u}{\partial y} \right|^{n+1} \right) + \frac{\sigma B_0^2}{T_\infty} u^2, \quad (13)$$

$$N_G = \frac{S_G}{S_0} \text{ where } S_0 = \frac{k(\Delta T)^2}{L^2 T_\infty}$$

$$N_G = \left( \frac{Re_b}{2} \right)^{\frac{2}{n+1}} (\theta')^2 + \frac{Br}{\Omega} \left[ \left( \frac{Re_b}{2} \right)^{\frac{2}{n+1}} f'' + \frac{Re_a}{2} |f''|^{n+1} \right] + \frac{M Br Re_a}{\Omega} (f')^2$$

where,  $Br = \frac{a u_w^2}{k \Delta T} = \frac{a u_0^2}{k T_0}$  is the Brinkman number,  $\Omega = \frac{\Delta T}{T_\infty}$  is the dimensionless temperature gradient. In addition, the Bejan number  $Be$  is introduced to check the domination of the heat transfer part over the fluid friction part along MHD flow. This dimensionless quantity is defined as:

$$Be = \frac{\left( \frac{Re_b}{2} \right)^{\frac{2}{n+1}}}{N_G} (\theta')^2 \quad (14)$$

### 4 Numerical method

Here, the numerical solving technique for the governing nonlinear Eqs. (9)-(12) with boundary conditions Eq. (13) are described. According to Saleem et al. [Saleem and Abd El-Aziz (2019); Abd El-Aziz and Saleem (2019)], the Runge-Kutta Fehlberg method with shooting technique is used to solve the governing nonlinear equations as:

First: we set:

$$y_1 = f, \quad y_2 = f', \quad y_3 = f'' \quad (15)$$

$$y_4 = \theta, \quad y_5 = \theta'$$

Second: The governing nonlinear equations are transformed into first order differential equations:

$$y_3' = \frac{2}{2A + n|y_3|^{n-1}} \left( y_2^2 - \left( \frac{2n-1}{n+1} \right) y_1 y_3 + M y_2 \right) \quad (16)$$

$$y_5' = Pr \left( 2y_2 y_4 - \left( \frac{2n-1}{n+1} \right) y_1 y_5 - M Ec y_2^2 - Ec \left( A y_3^2 + \frac{1}{2} |y_3|^{n+1} \right) \right) \quad (17)$$

with the boundary conditions:

$$\begin{aligned} y_1(0) &= 0, y_2(0) = 1 + \lambda(2A + |y_3|^{n-1})y_3(0), \\ y_3(0) &= \varepsilon_1, y_4(0) = \varepsilon_2 \\ y_5(0) &= -\gamma(1 - y_4(0)), \end{aligned} \quad (18)$$

Third: Step size of the numerical method is  $\Delta\eta = 0.001$ . And the computed values at  $\eta_\infty$  are fixed by Newton-Raphson method.

Finally, the repeat procedure is continuing until getting the results with correction up to  $10^{-6}$ .

## 5 Results and discussion

In order to get definite perception of the current physical problem, the velocity profile  $f'$ , temperature profile  $\theta$ , local entropy generation number  $N_G$  and Bejan number  $Be$  profiles are displayed under the effects of magnetic field parameter, local slip parameter  $\lambda$ , generalized Biot number  $\gamma$ , Sisko fluid material parameter, Eckert number, Prandtl number and Brinkman number  $Br$  at two values of power law index. The ranges the physical parameters are: magnetic field parameter ( $0 \leq M \leq 1.0$ ), material parameter ( $0.2 \leq A \leq 2.0$ ), local slip parameter ( $0 \leq \lambda \leq 0.4$ ), Eckert number ( $0 \leq Ec \leq 0.4$ ), Prandtl number ( $0.71 \leq Pr \leq 5.0$ ), generalized Biot number ( $0.1 \leq \gamma < \infty$ ), Brinkman number  $Br$  ( $1 \leq Br \leq 3$ ) and power-law index ( $n = 0.5, 1.5$ ).

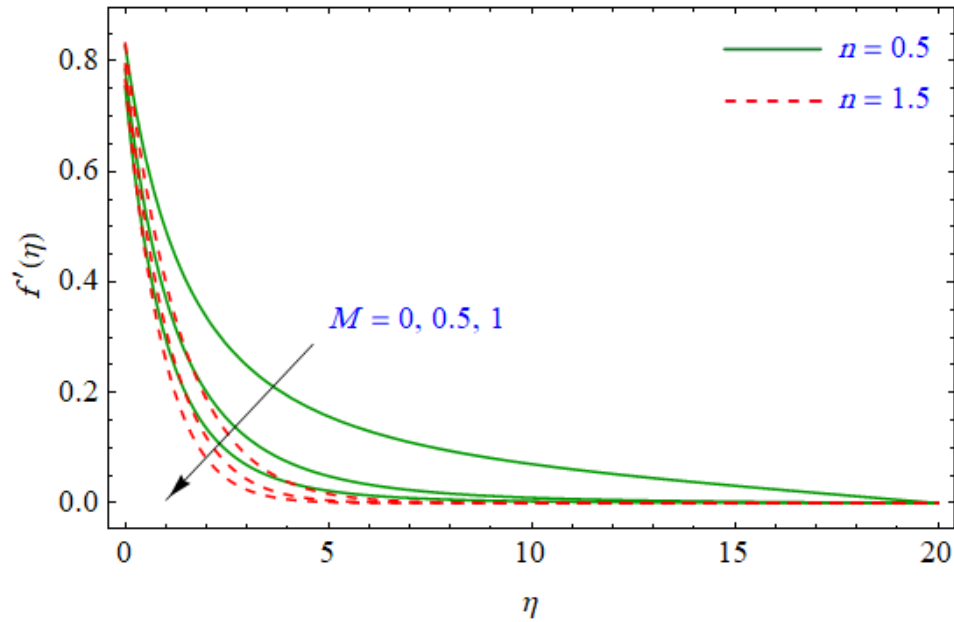


**Figure 2:** Velocity profiles under the effects of magnetic field parameter  $M$  at two values of power law index  $n=0.5$  and  $n=1.5$

Fig. 2 depicts the effects of magnetic field parameter  $M$  on the velocity profiles at two values of power law index  $n=0.5$  and  $n=1.5$ . Physically, as the magnetic field parameter increases, higher Lorentz forces were obtained which yield more resistance between the fluid particles and then the velocity profiles are decrease. In addition, the velocity profiles decrease and the boundary layer thickness is shrinking as the power law index increases from 0.5 to 1.5. Fig. 3 presents the temperature profiles under the effects of magnetic field parameter  $M$  at two values of power law index  $n=0.5$  and  $n=1.5$ . It is observed that, the temperature profiles as well as isothermal boundary layer thickness are increase according to an increase on magnetic field parameter. In addition, the power law  $n$  index plays an important role on controlling the thickness of the thermal boundary layer and their profiles. The temperature profiles and thermal boundary layer thickness are decrease as the power law index increases from 0.5 to 1.5.

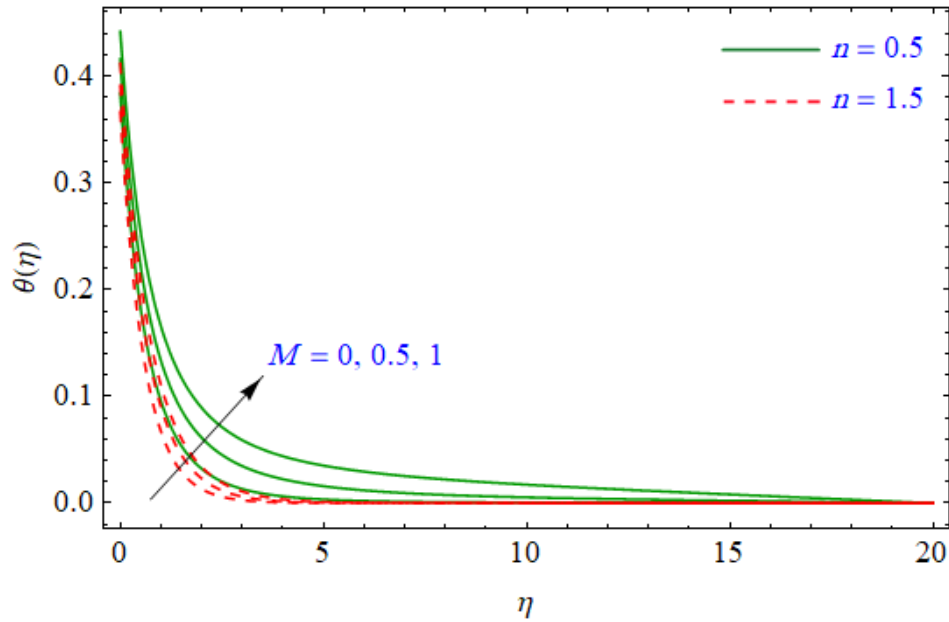


**Figure 3:** Temperature profiles under the effects of magnetic field parameter  $M$  at two values of power law index  $n=0.5$  and  $n=1.5$

Fig. 4 shows the temperature profiles under the effects of generalized Biot number  $\gamma$  at two values of power law index  $n=0.5$  and  $n=1.5$ . Here, the temperature profiles are increase as the generalized Biot number  $\gamma$  increases. Figs. 5 and 6 show the velocity and temperature profiles under the effects of material parameter  $A$  at two values of power law index  $n=0.5$  and  $n=1.5$ . According to an increase on the material parameter, the velocity profiles are increase, while the temperature profiles are decrease. The reason returns to the definition of material parameter  $A$ , at larger  $A$ , the shear rate of viscosity decreases which allows more fluid motion.

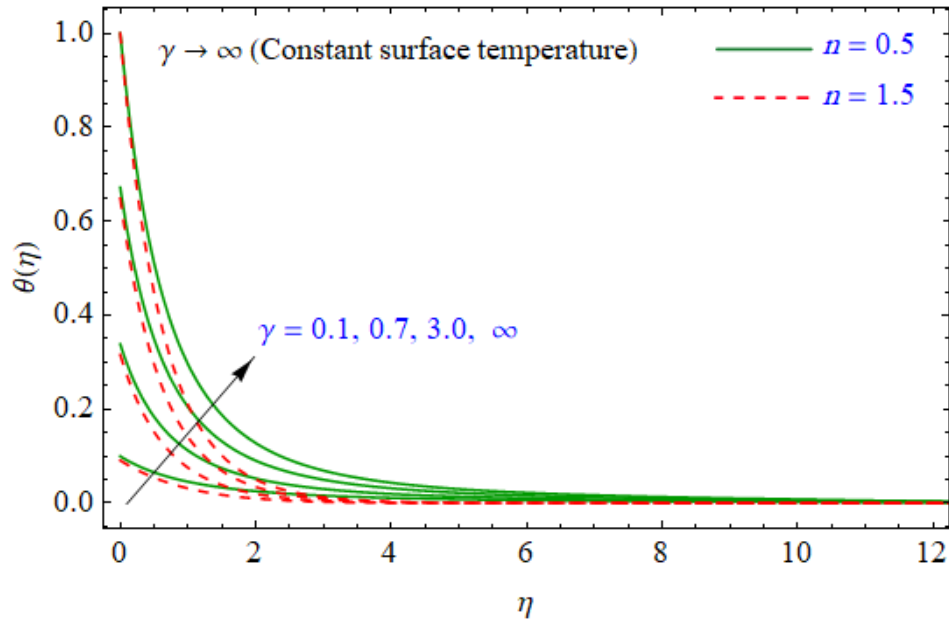


Figure 4: Temperature profiles under the effects of generalized Biot number  $\gamma$  at two values of power law index  $n=0.5$  and  $n=1.5$

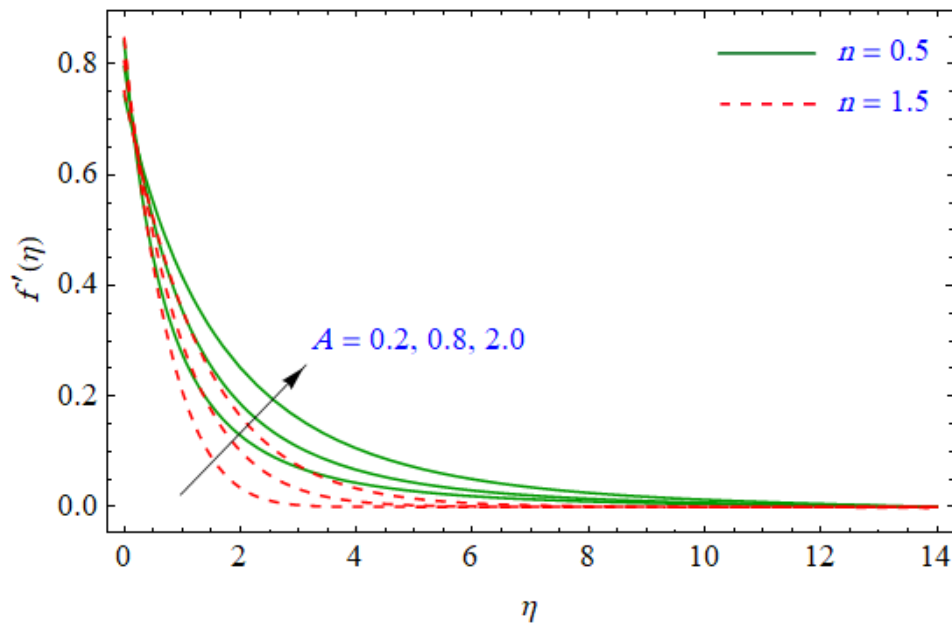
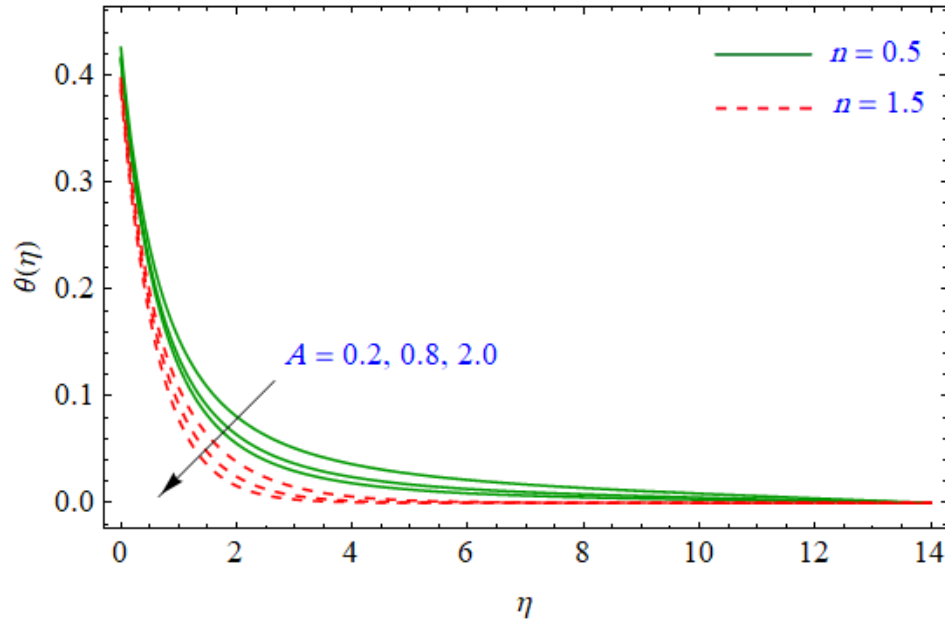


Figure 5: Velocity profiles under the effects of material parameter  $A$  at two values of power law index  $n=0.5$  and  $n=1.5$



**Figure 6:** Temperature profiles under the effects of material parameter  $A$  at two values of power law index  $n=0.5$  and  $n=1.5$

Figs. 7 and 8 present the velocity and temperature profiles under the effects of local slip parameter  $\lambda$  at two values of power law index  $n=0.5$  and  $n=1.5$ . It is seen that, an increase of local slip parameter  $\lambda$  leads to a decrease on the velocity profiles and an increase on the temperature profiles. Figs. 9 and 10 show the temperature profiles under the effects of Eckert number  $Ec$  and Prandtl number  $Pr$  at two values of power law index  $n=0.5$  and  $n=1.5$ . In these figures, the temperature profiles are increase as the Eckert number increases. These enhancements on the temperature return to that  $\theta(\eta)$  is an increasing function of  $Ec$ . Moreover, Eckert number convert the mechanical energy to thermal energy and hence the temperature enhances. Since, the Prandtl number is the ratio between the momentum diffusivity to thermal diffusivity. Then, it can control the momentum and thermal boundary layer thickness. Physically, the thermal diffusivity reduces for higher Prandtl number ( $0.71 \leq Pr \leq 5.0$ ). Hence, the temperature profiles are decrease as the Prandtl number increases.

It is found that, all of the previous figures depict that both of the velocity and temperature profiles are higher for the shear thinning fluids ( $n < 1$ ).

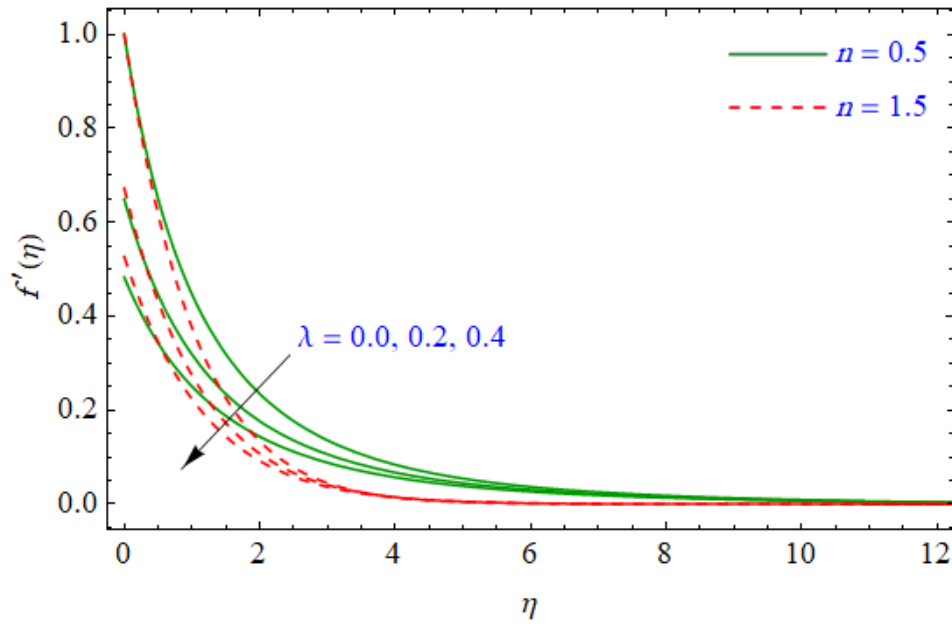


**Figure 7:** Velocity profiles under the effects of local slip parameter  $\lambda$  at two values of power law index  $n=0.5$  and  $n=1.5$

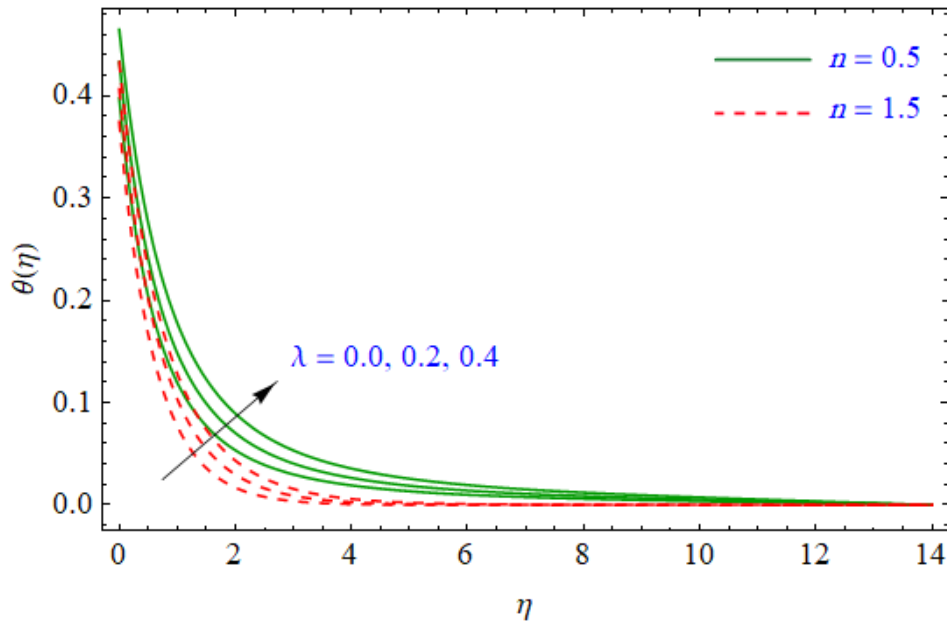


**Figure 8:** Temperature profiles under the effects of local slip parameter  $\lambda$  at two values of power law index  $n=0.5$  and  $n=1.5$

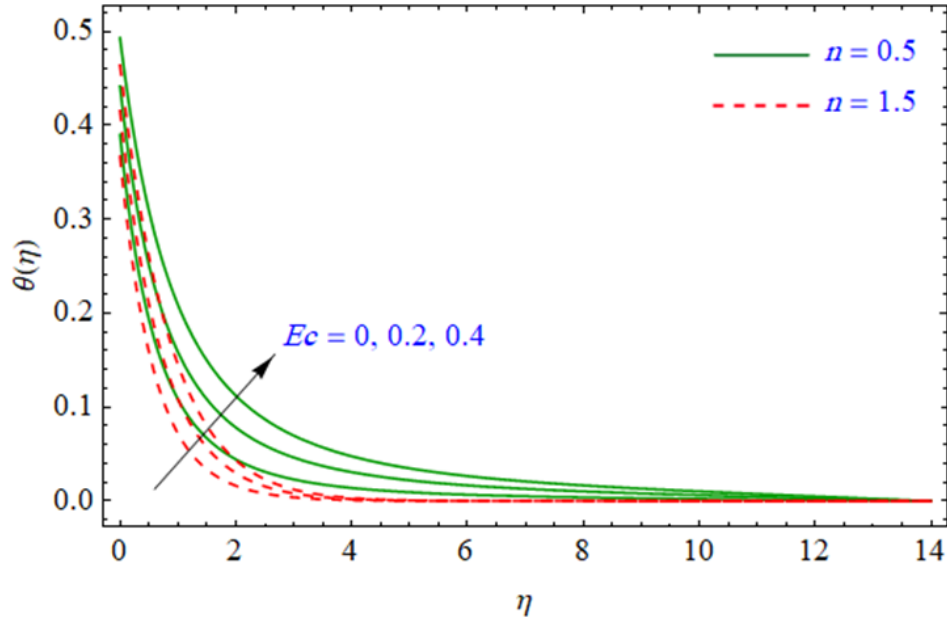


**Figure 9:** Temperature profiles under the effects of Eckert number  $Ec$  at two values of power law index  $n=0.5$  and  $n=1.5$

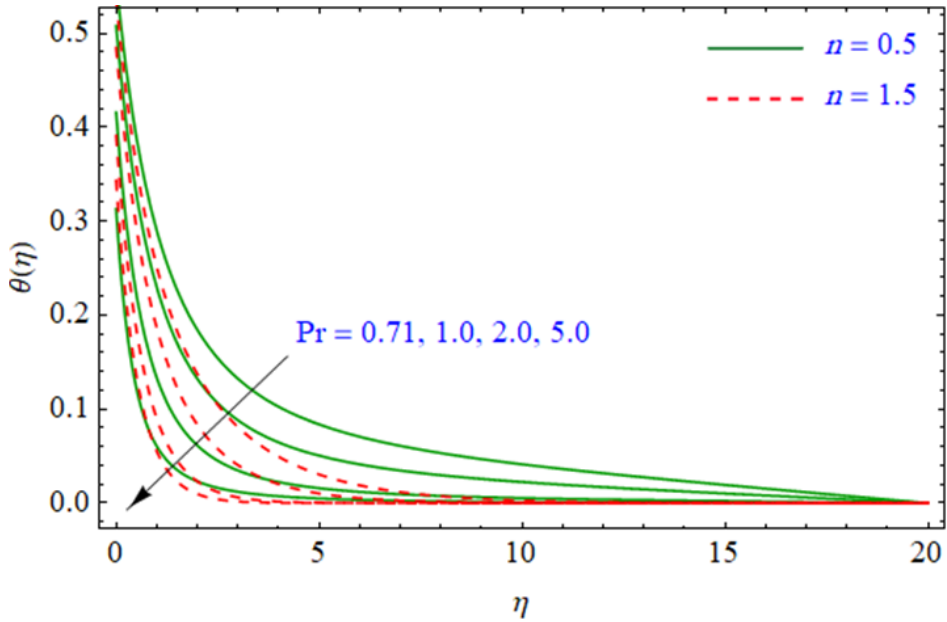


**Figure 10:** Temperature profiles under the effects of Prandtl number  $Pr$  at two values of power law index  $n=0.5$  and  $n=1.5$

Figs. 11-20 show the profiles of the local entropy generation number and Bejan number  $Be$  under the effects of generalized Biot number  $\gamma$ , magnetic field parameter  $M$ ,

material parameter  $A$ , local slip parameter  $\lambda$  and Brinkman number  $Br$  at two values of power law index  $n=0.5$  and  $n=1.5$ . The effects of the generalized Biot number  $\gamma$  at two values of power law index  $n=0.5$  and  $n=1.5$  on the local entropy generation number  $N_G$  and Bejan number are shown in Figs. 11 and 12. As the generalized Biot number  $\gamma$  increases, the profiles of local entropy generation number  $N_G$  and Bejan number  $Be$  are increase. In addition, the higher values of  $N_G$  and  $Be$  are obtained at higher power law index ( $n = 1.5$ ). In Figs. 13 and 14, an increase on the magnetic field parameter leads to an increase on the local entropy generation number  $N_G$  and a decrease on the Bejan number  $Be$ . The physical meaning returns to higher values of Lorentz force which yield more resistance and then more disturbance in the system so  $N_G$  increases. Figs. 15 and 16 depict the effects of material parameter  $A$  on the local entropy generation number  $N_G$  and Bejan number  $Be$  under the effects of at two values of power law index  $n=0.5$  and  $n=1.5$ . The local entropy generation number  $N_G$  decreases as material parameter  $A$  increases and there are almost no changes under the effects of power law index  $n$  at this case. The Bejan number  $Be$  increases as material parameter  $A$  increases and its higher values at higher power law index ( $n = 1.5$ ). The local entropy generation number  $N_G$  decreases as  $\lambda$  increases and it increases as  $Br$  increases. The Bejan number  $Be$  increases as  $\lambda$  increases and it decreases as  $Br$  as shown in Figs. 17-20. In these figures, the local entropy generation number and Bejan number have a slight more values at higher power law index ( $n = 1.5$ ).

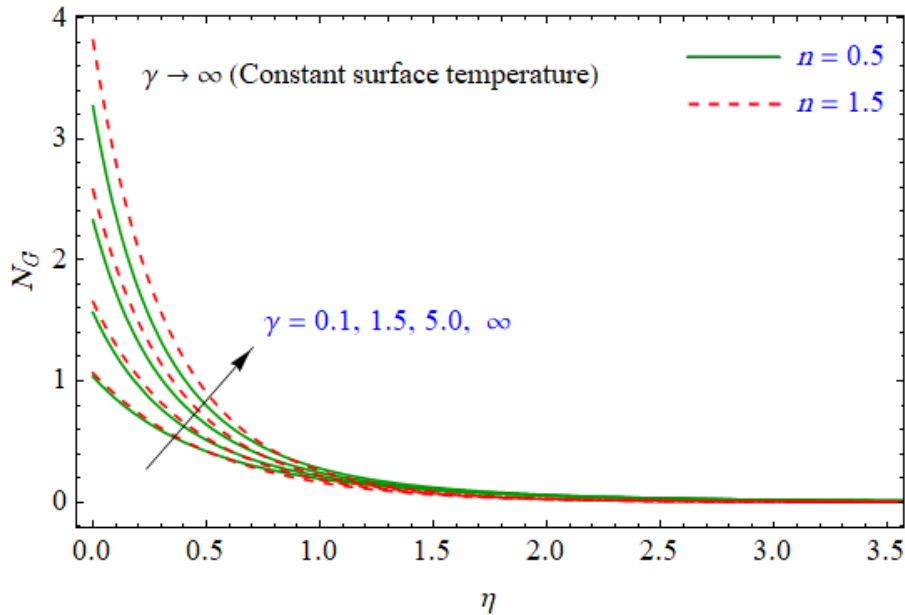


**Figure 11:** Local entropy generation number  $N_G$  under the effects of generalized Biot number  $\gamma$  at two values of power law index  $n=0.5$  and  $n=1.5$

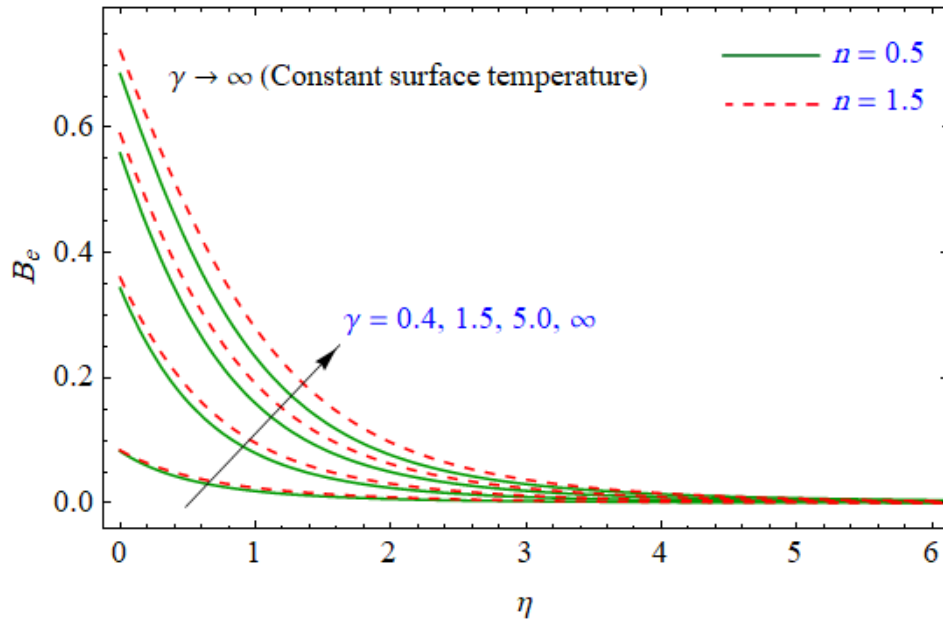


**Figure 12:** Profiles of the Bejan number  $Be$  under the effects of generalized Biot number  $\gamma$  at two values of power law index  $n=0.5$  and  $n=1.5$

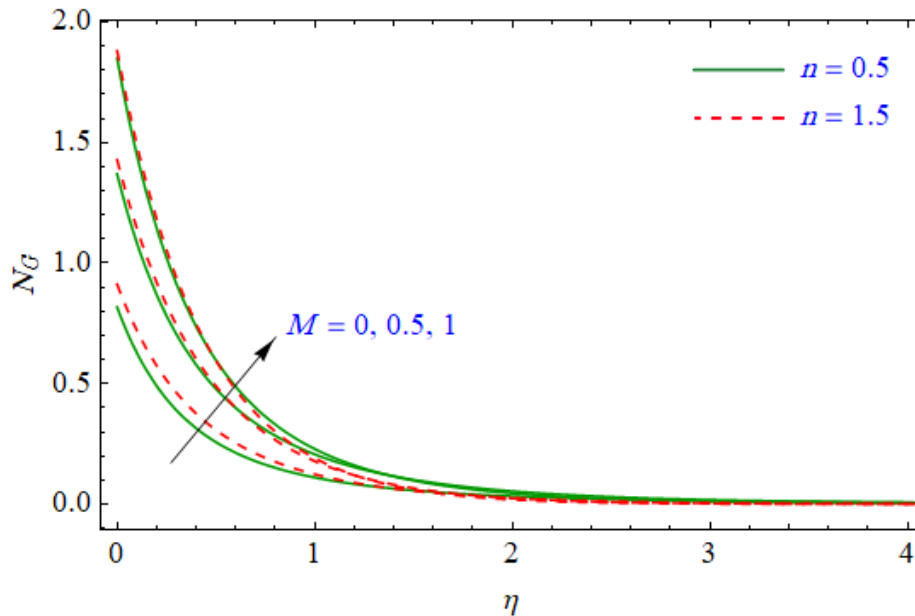


**Figure 13:** Local entropy generation number  $N_G$  under the effects of magnetic field parameter  $M$  at two values of power law index  $n=0.5$  and  $n=1.5$

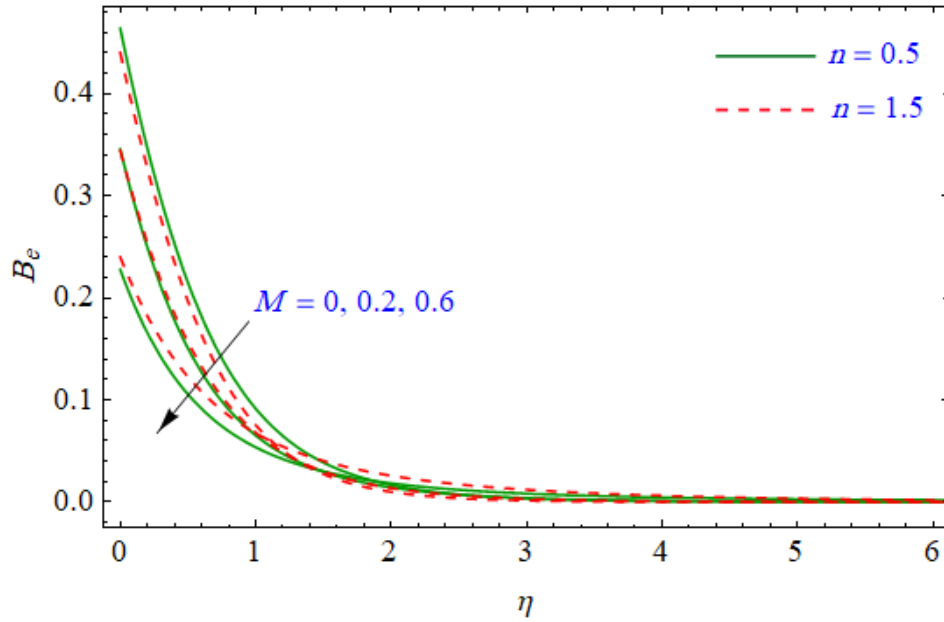


**Figure 14:** Profiles of the Bejan number  $Be$  under the effects of magnetic field parameter  $M$  at two values of power law index  $n=0.5$  and  $n=1.5$

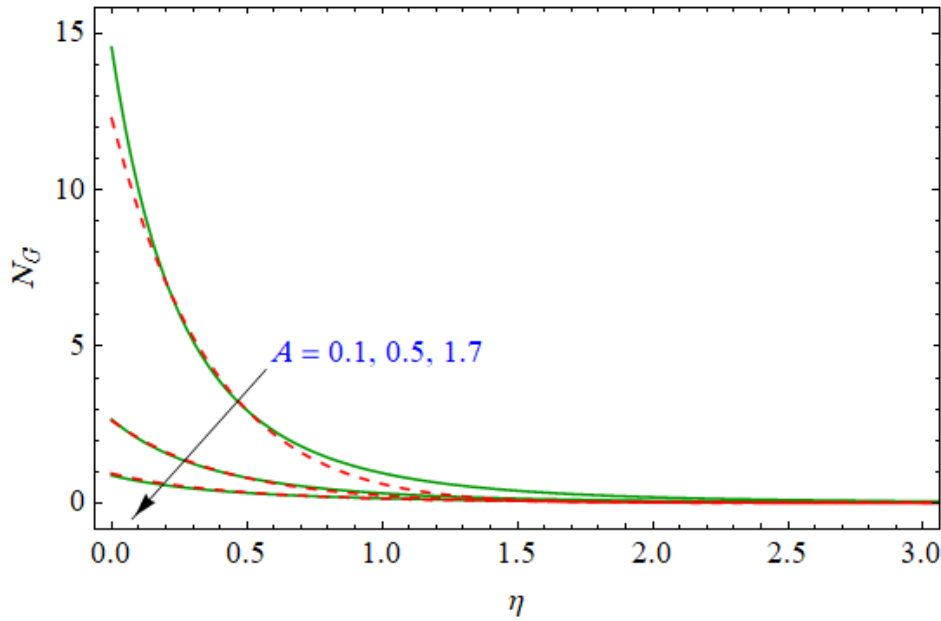


**Figure 15:** Local entropy generation number  $N_G$  under the effects of material parameter  $A$  at two values of power law index  $n=0.5$  and  $n=1.5$

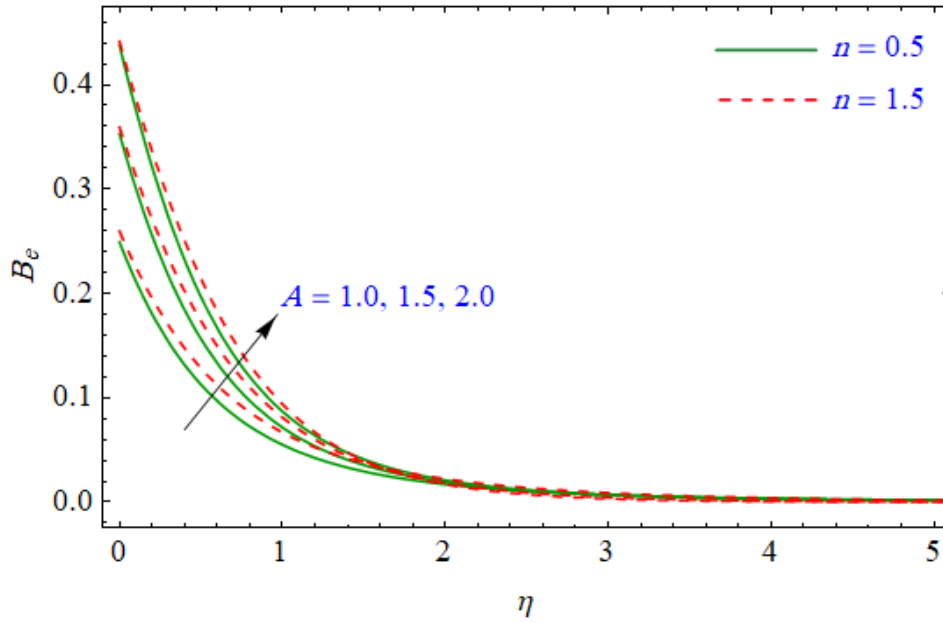


**Figure 16:** Profiles of the Bejan number  $Be$  under the effects of material parameter  $A$  at two values of power law index  $n=0.5$  and  $n=1.5$

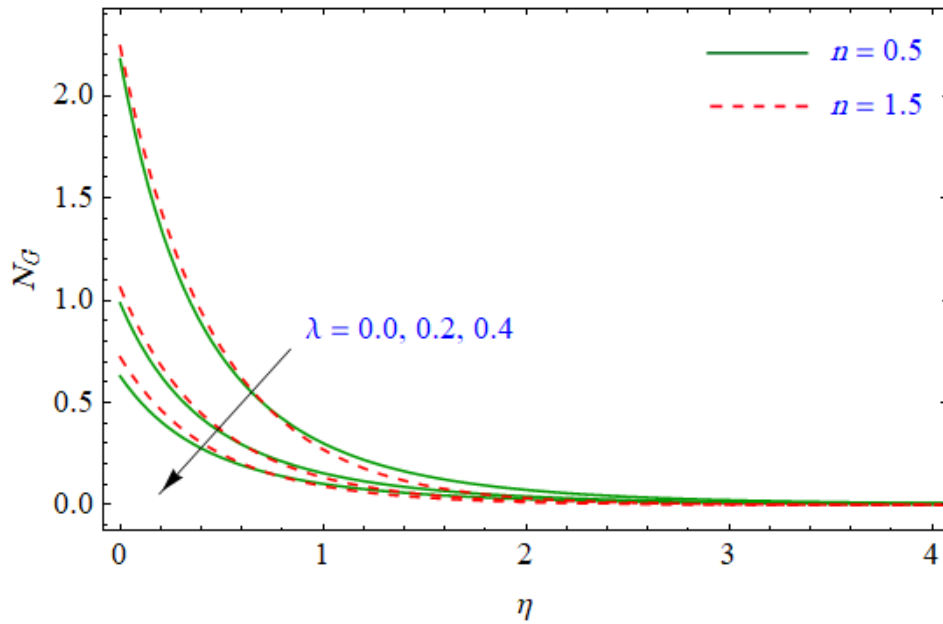


**Figure 17:** Local entropy generation number  $N_G$  under the effects of local slip parameter  $\lambda$  at two values of power law index  $n=0.5$  and  $n=1.5$

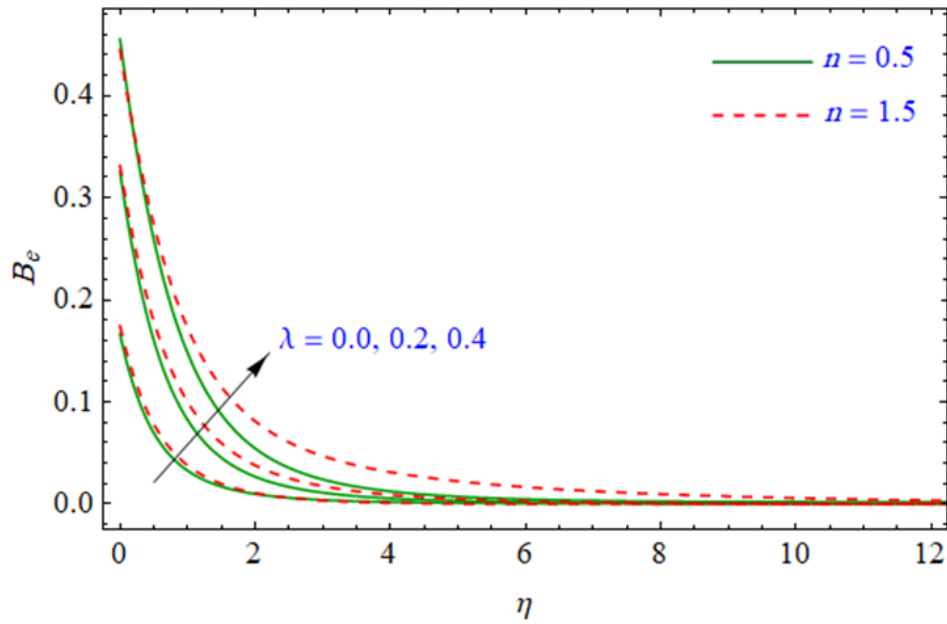


**Figure 18:** Profiles of the Bejan number  $Be$  under the effects of local slip parameter  $\lambda$  at two values of power law index  $n=0.5$  and  $n=1.5$

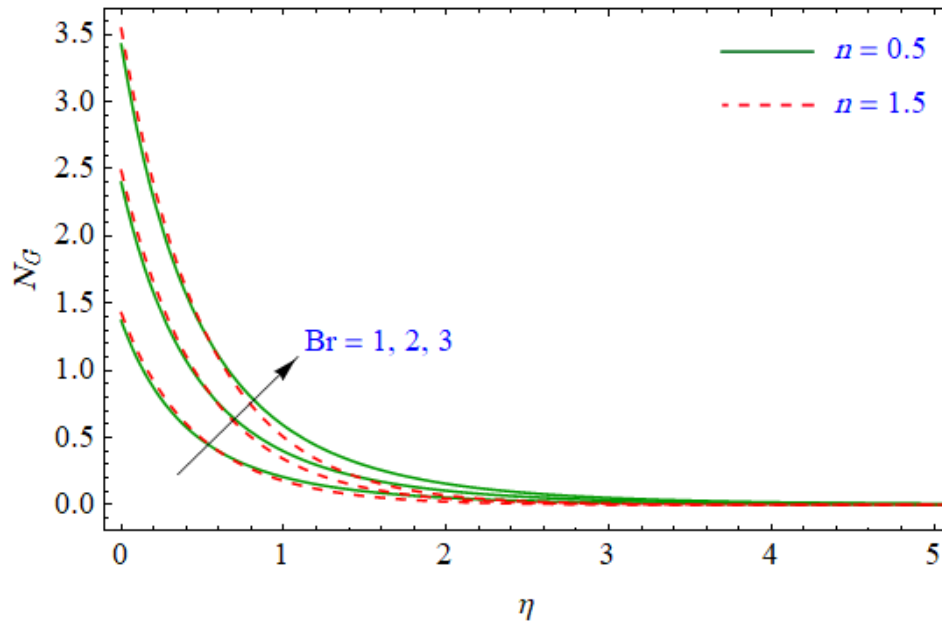


**Figure 19:** Local entropy generation number  $N_G$  under the effects of Brinkman number  $Br$  at two values of power law index  $n=0.5$  and  $n=1.5$

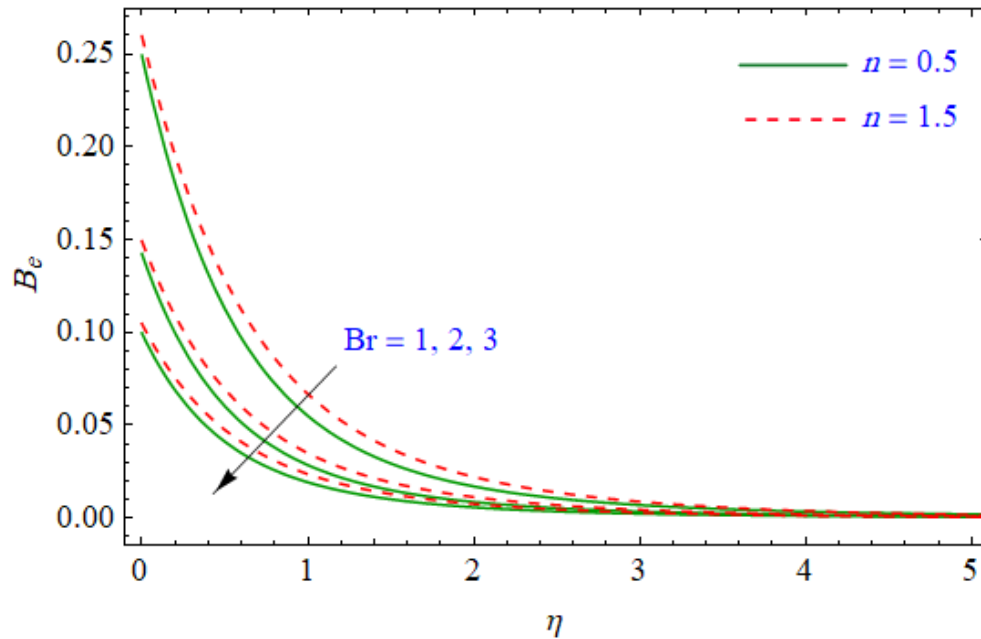


**Figure 20:** Profiles of the Bejan number  $Be$  under the effects of Brinkman number  $Br$  at two values of power law index  $n=0.5$  and  $n=1.5$

Tab. 1 presents the values of local skin friction coefficient for different values of  $M$ ,  $A$  and  $\lambda$ . In this table, the local skin friction coefficient increases as the magnetic field parameter  $M$  and material parameter  $A$  are increase and it decreases as local slip parameter  $\lambda$  increases. The values of the local skin friction coefficient are higher at lower power law index ( $n = 0.5$ ) for all of the cases. Tab. 2 presents the values of the local Nusselt number for different values of  $M$ ,  $A$ ,  $\lambda$ ,  $\gamma$ ,  $Ec$  and  $Pr$ . In this table, the local Nusselt number decreases as magnetic field parameter  $M$ , local slip parameter  $\lambda$  and Eckert number  $Ec$  are increase. While, the local Nusselt number increases as Sisko-fluid material parameter  $A$ , generalized Biot number  $\gamma$  and Prandtl number  $Pr$  are increase. For all of the cases, the local Nusselt number has higher values at higher power law index ( $n = 1.5$ ).

**Table 1:** Values of local skin friction coefficient  $-\left(\frac{Re_b}{2}\right)^{\frac{1}{n+1}} C_f$  for different values of  $M$ ,  $A$  and  $\lambda$

$M$	$A$	$\lambda$	$-\left(\frac{Re_b}{2}\right)^{\frac{1}{n+1}} C_f$	
			$n = 0.5$	$n = 1.5$
<b>0.0</b>	1.0	0.1	1.72671	1.68459
<b>0.5</b>			2.15530	2.05678
<b>1.0</b>			2.46294	2.34578
0.5	<b>0.2</b>		1.59445	1.53366
	<b>0.8</b>		2.04627	1.94618
	<b>2.0</b>		2.56732	2.48979
		<b>0.0</b>	2.82742	2.83699
		<b>0.2</b>	1.75579	1.63826
		<b>0.4</b>	1.29243	1.18343

**Table 2:** Values of the local Nusselt number  $\left(\frac{Re_b}{2}\right)^{-\frac{1}{n+1}} Nu_x$  for different values of  $M$ ,  $A$ ,  $\lambda$ ,  $\gamma$ ,  $Ec$  and  $Pr$

$M$	$A$	$\lambda$	$\gamma$	$Ec$	$Pr$	$\left(\frac{Re_b}{2}\right)^{-\frac{1}{n+1}} Nu_x$	
						$n = 0.5$	$n = 1.5$
<b>0.0</b>	1.0	0.1	1.0	0.1	2.0	0.615751	0.633529
<b>0.5</b>						0.584125	0.608885
<b>1.0</b>						0.558153	0.588077
0.5	<b>0.2</b>					0.574262	0.602873
	<b>0.8</b>					0.583166	0.608356
	<b>2.0</b>					0.585395	0.613924
		<b>0.0</b>				0.602178	0.625537
		<b>0.2</b>				0.566617	0.593439
		<b>0.4</b>				0.535260	0.567009
			<b>0.1</b>			0.090027	0.090902
			<b>0.7</b>			0.463094	0.478930
			<b>3.0</b>			0.984263	1.053603
				<b>0.0</b>		0.609808	0.633139
				<b>0.2</b>		0.558436	0.584632
				<b>0.4</b>		0.507064	0.536125
					<b>0.71</b>	0.443020	0.463558
					<b>1.0</b>	0.491898	0.515105
					<b>2.0</b>	0.584125	0.608885

## 5 Conclusion

This work investigated the effects of the magnetic field on entropy generation during fluid flow and heat transfer of a Sisko-fluid over an exponentially stretching surface. The nonlinear partial differential equations are transformed into dimensionless similar equations. The Runge-Kutta-Fehlberg method is used to solve the dimensionless similar equations. The control parameters including magnetic field parameter  $M$ , material parameter  $A$ , local slip parameter  $\lambda$ , Brinkman number  $Br$ , generalized Biot number  $\gamma$  and Prandtl number  $Pr$  have been considered. The effects of these parameters on the velocity and temperature profiles as well as the local skin-friction coefficient and local Nusselt are explored. The main findings of this work are reported:

- An extra magnetic field parameter makes higher Lorentz force that suppresses the velocity.
- Temperature rises for larger  $M$ ,  $\gamma$ ,  $\lambda$  and  $Ec$ , while it decays for larger  $Pr$  and  $A$ .
- For shear thinning fluids ( $n < 1$ ), the temperature dominates and the velocity rises.
- Local entropy generation number is more for largerfor , while it decays  $Brand M$ ,  $\gamma$  larger  $A$  and  $\lambda$ .
- Bejan number increases as  $\gamma$ ,  $A$  and  $\lambda$  are increase and it decreases as  $M$  and  $Br$  are increase.
- The local skin friction coefficient increases as  $M$  and  $A$  are increase and it decreases as  $\lambda$  increases.
- The local Nusselt number decreases as  $M$ ,  $\lambda$  and  $Ec$  are increase, while it increases as  $A$ ,  $\gamma$  and  $Pr$  are increase.

**Acknowledgment:** The authors extend their appreciation to the Deanship of Scientific Research at King Khalid University for funding this work through Big Group Research Project under grant number (R.G.P2/16/40).

## References

- Abd El-Aziz, M.; Afify, A. A.** (2016): Lie group analysis of hydromagnetic flow and heat transfer of a power-law fluid over stretching surface with temperature-dependent viscosity and thermal conductivity. *International Journal of Modern Physics C*, vol. 27, no. 12, 1650150.
- Abd El-Aziz, M.; Saleem, S.** (2019): Numerical simulation of entropy generation for power-law liquid flow over a permeable exponential stretched surface with variable heat source and heat flux. *Entropy*, vol. 21, no. 5, pp. 1-19.
- Afify, A. A.; Abd El-Aziz, M.** (2017): Lie group analysis of flow and heat transfer of non-Newtonian nanofluid over a stretching surface with convective boundary condition. *Pramana*, vol. 88, no. 2, pp. 1-31.
- Ahmed, S. E.; Aly, A. M.; Mansour, M. A.** (2015): Mhd mixed bioconvection stagnation point flow of nanofluids towards a stretching surface. *Journal of Nanofluids*, vol. 4, no. 4, pp. 528-535.

**Ali, N.; Zaman, A.; Sajid, M.** (2014): Unsteady blood flow through a tapered stenotic artery using Sisko model. *Computers & Fluids*, vol. 101, pp. 42-49.

**Bachok, N.; Ishak, A.; Pop, I.** (2012): Boundary layer stagnation-point flow and heat transfer over an exponentially stretching/shrinking sheet in a nanofluid. *International Journal of Heat and Mass Transfer*, vol. 55, no. 25-26, pp. 8122-8128.

**Battaller, R. C.** (2008): Similarity solutions for flow and heat transfer of a quiescent fluid over a nonlinearly stretching surface. *Journal of Materials Processing Technology*, vol. 203, no. 1-3, pp. 176-183.

**Chamkha, A. J.; Mansour, M. A.; Aly, A. M.** (2011): Unsteady mhd free convective heat and mass transfer from a vertical porous plate with hall current, thermal radiation and chemical reaction effects. *International Journal for Numerical Methods in Fluids*, vol. 65, no. 4, pp. 432-447.

**Chamkha, A. J.; Aly, A. M.** (2010): Mhd free convection flow of a nanofluid past a vertical plate in the presence of heat generation or absorption effects. *Chemical Engineering Communications*, vol. 198, no. 3, pp. 425-441.

**Chamkha, A. J.; Aly, A. M.** (2010): Heat and mass transfer in a stagnation-point flow of a polar fluid towards a stretching surface in porous media in the presence of sores, dufour and chemical reaction effects. *Chemical Engineering Communications*, vol. 198, no. 2, pp. 214-234.

**Chamkha, A. J.; Aly, A. M.; Al-Mudhaf, H. F.** (2011): Laminar mhd mixed convection flow of a nanofluid along a stretching permeable surface in the presence of heat generation or absorption effects. *International Journal of Microscale and Nanoscale Thermal and Fluid Transport Phenomena*, vol. 2, no. 1, pp. 1-51.

**Chamkha, A. J.; Aly, A. M.; Mansour, M. A.** (2010): Similarity solution for unsteady heat and mass transfer from a stretching surface embedded in a porous medium with suction/injection and chemical reaction effects. *Chemical Engineering Communications*, vol. 197, no. 6, pp. 846-858.

**Ghadikolaei, S. S.; Hosseinzadeh, K.; Ganji, D. D.** (2018): Mhd radiative boundary layer analysis of micropolar dusty fluid with graphene oxide (Go)-engine oil nanoparticles in a porous medium over a stretching sheet with joule heating effect. *Powder Technology*, vol. 338, pp. 425-437.

**Hayat, T.; Khan, M. I.; Qayyum, S.; Khan, M. I.; Alsaedi, A.** (2018): Entropy generation for flow of Sisko fluid due to rotating disk. *Journal of Molecular Liquids*, vol. 264, pp. 375-385.

**Hayat, T.; Shafiq, A.; Alsaedi, A.; Awais, M.** (2013): Mhd axisymmetric flow of third grade fluid between stretching sheets with heat transfer. *Computers & Fluids*, vol. 86, pp. 103-108.

**Hsiao, K. L.** (2016): Stagnation electrical mhd nanofluid mixed convection with slip boundary on a stretching sheet. *Applied Thermal Engineering*, vol. 98, pp. 850-861.

**Ibrahim, W.; Shankar, B.; Nandeppanavar, M. M.** (2013): Mhd stagnation point flow and heat transfer due to nanofluid towards a stretching sheet. *International Journal of Heat and Mass Transfer*, vol. 56, no. 1-2, pp. 1-9.

- Khan, M.; Munawar, S.; Abbasbandy, S.** (2010): Steady flow and heat transfer of a Sisko fluid in annular pipe. *International Journal of Heat and Mass Transfer*, vol. 53, no. 7-8, pp. 1290-1297.
- Khan, M. I.; Hayat, T.; Alsaedi, A.; Qayyum, S.; Tamoor, M.** (2018): Entropy optimization and quartic autocatalysis in mhd chemically reactive stagnation point flow of Sisko nanomaterial. *International Journal of Heat and Mass Transfer*, vol. 127, pp. 829-837.
- Khan, M. I.; Hayat, T.; Qayyum, S.; Khan, M. I.; Alsaedi, A.** (2018): Entropy generation (irreversibility) associated with flow and heat transport mechanism in Sisko nanomaterial. *Physics Letters A*, vol. 382, no. 34, pp. 2343-2353.
- Khan, M. I.; Qayyum, S.; Hayat, T.; Alsaedi, A.; Khan, M. I.** (2018): Investigation of Sisko fluid through entropy generation. *Journal of Molecular Liquids*, vol. 257, pp. 155-163.
- Khan, W. A.; Khan, M.; Alshomrani, A. S.; Ahmad, L.** (2016): Numerical investigation of generalized Fourier's and Fick's laws for Sisko fluid flow. *Journal of Molecular Liquids*, vol. 224, pp. 1016-1021.
- Mabood, F.; Khan, W. A.; Ismail, A. I. M.** (2015): Mhd boundary layer flow and heat transfer of nanofluids over a nonlinear stretching sheet: a numerical study. *Journal of Magnetism and Magnetic Materials*, vol. 374, pp. 569-576.
- Mansour, M. A.; El-Anssary, N. F.; Aly, A. M.** (2008): Effects of chemical reaction and thermal stratification on mhd free convective heat and mass transfer over a vertical stretching surface embedded in a porous media considering soret and dufour numbers. *Chemical Engineering Journal*, vol. 145, no. 2, pp. 340-345.
- Mekheimer, K. S.; El Kot, M.** (2012): Mathematical modelling of unsteady flow of a Sisko fluid through an anisotropically tapered elastic arteries with time-variant overlapping stenosis. *Applied Mathematical Modelling*, vol. 36, no. 11, pp. 5393-5407.
- Nadeem, S.; Akbar, N. S.** (2010): Peristaltic flow of Sisko fluid in a uniform inclined tube. *Acta Mechanica Sinica*, vol. 26, no. 5, pp. 675-683.
- Raizah, Z. A.** (2017): Mhd mixed bioconvection stagnation point flow of a nanofluid towards stretching surfaces with viscous dissipation and joule heating effects. *Computational Thermal Sciences: An International Journal*, vol. 9, no. 5, pp. 467-481.
- Saleem, S.; Abd El-Aziz, M.** (2019): Entropy generation and convective heat transfer of radiated non-Newtonian power-law fluid past an exponentially moving surface under slip effects. *European Physical Journal Plus*, vol. 134, no. 4, pp. 184.
- Sisko, A.** (1958): The flow of lubricating greases. *Industrial & Engineering Chemistry*, vol. 50, no. 12, pp. 1789-1792.
- Sparrow, E. M.; Cess, R. D.** (1961): The effect of a magnetic field on free convection heat transfer. *International Journal of Heat and Mass Transfer*, vol. 3, no. 4, pp. 267-274.
- Tanveer, A.; Hayat, T.; Alsaedi, A.; Ahmad, B.** (2017): Mixed convective peristaltic flow of Sisko fluid in curved channel with homogeneous-heterogeneous reaction effects. *Journal of Molecular Liquids*, vol. 233, pp. 131-138.

**Uddin, M. J.; Khan, W. A.; Ismail, A. I.** (2012): Mhd free convective boundary layer flow of a nanofluid past a flat vertical plate with newtonian heating boundary condition. *PLoS One*, vol. 7, no. 11, e49499.

**Veera K. M.; Reddy, G. M.** (2018): Mhd free convective boundary layer flow through porous medium past a moving vertical plate with heat source and chemical reaction. *Materials Today: Proceedings*, vol. 5, no. 1(Part 1), pp. 91-98.